Published in final edited form as:
Carbohydr Polym. 2015 March 6; 117: 964–972. doi:10.1016/j.carbpol.2014.10.022.

Inulin crystal initiation via a glucose-fructose cross-link of adjacent polymer chains: atomic force microscopy and static molecular modelling

Peter D. Cooper[a,b,*], **K. Harinda Rajapaksha**[a], **Thomas G. Barclay**[c], **Milena Ginic-Markovic**[c], **Andrea R. Gerson**[c], and **Nikolai Petrovsky**[a,d,#]

[a]Vaxine Pty Ltd, Flinders Medical Centre, Bedford Park, SA, Australia 5042

[b]Cancer Research Laboratory, Australian National University Medical School at The Canberra Hospital, Garran, ACT, Australia 2605; and John Curtin School of Medical Research, Australian National University, Acton, ACT, Australia 2601

[c]Mawson Institute, University of South Australia, Mawson Lakes, SA, Australia 5095

[d]Department of Endocrinology, Flinders Medical Centre/Flinders University, Bedford Park, SA, Australia, 5042

Abstract

Semi-crystalline microparticles of inulin (MPI) have clinical utility as potent human vaccine adjuvants but their relevant surface structure and crystal assembly remain undefined. We show inulin crystal surfaces to resemble multi-layered, discoid radial spherulites resulting from very rapid formation of complex tertiary structures, implying directed crystal initiation. Physical and *in silico* molecular modelling of unit cells confirm steric feasibility of initiation by hydrogen-bonded cross-linking of terminal glucose to a fructose of another chain, mimicking bonding in sucrose crystals. A strong, chelate-like dual H-bond is proposed to compel the known antiparallel alignment of inulin chains. Such cross-linking would require one extra fructose per chain in the native inulin crystal, as observed. Completion of five H-bonded internal ring-domains would 'lock in' each new 6-fructose structural unit of each antiparallel helix pair to create a new isoform. All known properties of inulin isoforms follow readily from these concepts.

[*]Corresponding author. Tel:+61-2-62319926; Fax: +61-8-82045987; peter.cooper@anu.edu.au. [#]Author for proofs and reprints. Tel: +61-8-82044572; Fax: +61-8-82045987; nikolai.petrovsky@flinders.edu.au.

Chemical compounds studied in this article
Inulin from chicory (PubChem CID: 16219508); Fructose (PubChem CID: 5984); Sucrose (PubChem CID: 5988); L-Xylose (PubChem CID: 95259); Glycerol (PubChem CID: 753); Glucose (PubChem CID: 5793)

Conflict of interest statement
P.C., H.R. and N.P. are employees or consultants of Vaxine Pty Ltd.

Keywords

adjuvant; isoform; model; structure; vaccine

1. Introduction

Secondary structure in inulin plant fructans is well researched (Franck & De Leenheer, 2002). A family of linear, (2→1)-β-D-furanosyl glycosides with a single terminal glucose link as in sucrose comprises polymer chains of up to 100 fructose residues. The many applications of inulin (Barclay, Ginic-Markovic, Cooper & Petrovsky, 2010) include a stable semi-crystalline form termed microparticulate inulin (MPI) currently in advanced human and veterinary clinical development as a vaccine adjuvant. It is broadly effective as the commercially produced delta isoform Advax™ adjuvant (Gordon et al., 2012; Honda-Okubo, Saade & Petrovsky, 2012; Larena, Prow, Hall, Petrovsky & Lobigs, 2013; Petrovsky et al., 2013; Saade, Honda-Okubo, Trec & Petrovsky, 2013; see also Cooper, Barclay, Ginic-Markovic, & Petrovsky, 2013, 2014a; Cooper, Barclay, Ginic-Markovic, Gerson, & Petrovsky, 2014b). We here outline a model of MPI assembly and surface structure, known to be important for its adjuvant efficacy because dissolved inulin is immunologically inactive.

Different polymorphic forms of inulin exist, distinguished by their solubility and H-bonding strengths (Cooper & Petrovsky, 2011; Cooper et al., 2013). Differences in immune actions of these forms were also noted and remain a focus of ongoing research. They usually occur as isoforms, presenting the same thermal phenotypes but also including longer polymer chains and termed ‘plus-format’ preparations. All seven inulin isoforms, including five newly described ones, comprise a fixed incremental series in which each has greater H-bonding strength than its precursor. Each is characterized by its critical temperature (Tc), i.e. point of abrupt phase shift (solubilization in water) or by its dry melting point (MP) in modulated differential scanning calorimetry (Cooper et al., 2013). These properties and inulin’s known ability to form crystals (André, Mazeau et al., 1996) imply a crystalline or semi-crystalline nature for MPI. Their Tc and MP increase in a strikingly step-wise manner, a regularity suggesting that one energetic unit is being added to a preceding structure for each step in higher isoform creation. When new isoform isolates were each prepared to comprise only the chain lengths minimally defining each isoform (‘monoformat preparations’, Cooper et al., 2014b), regular increments were confirmed by number average degree of polymerization (DPn) assay, showing a step-wise addition of an energetic unit of 6 fructose residues per chain for each higher isoform (the highest isoform adding 12 such fructose residues). As the *d*-spacings of the X-ray diffraction patterns of all these seven isoforms were the same as those of André, Mazeau et al. (1996), each added energetic unit was equivalent to one crystal unit cell (Cooper et al., 2014b). Further, each isoform had one ‘extra’ fructose unit per chain, following the fructose DPn progression (6N +1) rather than 6N (N = unit cells).

We sought here static modelling approaches to resolve the way that individual inulin chains may assemble to form MPI isoform structures observed in atomic force microscopy (AFM),

and to characterise internal bonding of their unit cell, especially any role of the terminal glucose, a feature not previously considered (André, Mazeau et al., 1996).

2. Materials and Methods

2.1 Inulin

Inulin isoforms were sourced, prepared and handled as in Cooper et al., 2013.

2.2 Atomic force microscopy

AFM examined samples prepared from either clear solutions of inulin (5 μL, 50 mg mL^{-1}) allowed to crystallize on flat silicon wafers at room temperature (RT, ~20 ° C) or on aqueous dispersions of MPI diluted to 0.1 mg mL^{-1} and deposited (5 μL) onto a wafer. The samples were air-dried before imaging using a Digital Instruments Veeco Multimode Scanning Probe Microscopy system with a Nanoscope IV controller operating in standard tapping mode. The cantilevers used were Mikromasch NSC15 with spring constants between 30–60 N/m and resonant frequencies between 310–365 kHz. The data were acquired in air at RT using Nanoscope software (v8.10r1) and images analyzed with Veeco Nanoscope Analysis software (v. 1.20).

2.3 Physical structural model

Ball-and-stick plastic kits (Zometool Inc, Lakewood CO) comprise light-weight, hollow, symmetrical spheres 18.5 mm diameter with 62 geometrical holes at precise 2-, 3-, and 5-fold symmetries. Plastic struts locking into 3-fold holes allow reproducible lengths for C -C and C - O bonds (40.0 mm centre-to-centre) and correct bond angles. Two minor compromises are needed: 1. As C - C and C - O bond lengths are 1.52 Å and 1.42 Å, respectively, a scale is chosen (2.752 cm/Å) as a weighted average (1.45 Å) of the dimension-critical inulin helix backbone (- C - C - O -), where there are two C - O and one C - C bonds between furanose rings; 2. The Zometool holes do not permit rotable bonds, and so for such atoms (glycosidic oxygen, C1 and C6 carbons) two 5-fold symmetry holes are drilled out (3.5 mm bit) to admit the triangular pegs that can then be rotated. These permit dihedral bond angles of 108° close to the tetrahedral bond angles (109.5°). Glycosidic oxygen has ether links of 109–110° predicted by valence shell electron-pair repulsion theory.

The helical glycosidic backbone contains 18 rotable bonds per turn of the helix per unit cell proposed (André, Mazeau et al., 1996), conferring extreme flexibility. Accordingly, the glycosidic oxygen atoms are first immobilized on a scaffold of bamboo skewers (3 mm diameter) mounted in a wooden base at the apices of a regular hexagon of sides 8.35cm (3.03 Å), corresponding to Fig. 2 of André, Mazeau et al.(1996). The skewer heights fix each glycosidic oxygen 6.74 cm (2.45 Å) above its precursor, corresponding to an equal elevation for each fructose moiety. A process of ‘best-fit’ gives rotational angles (angles of André, Mazeau et al.) of $\phi = 68°$ (66°), $\psi = 159°$ (154.5°), $\omega = -87°$ (−81.8°), that allow both lateral and planar rotations of each furanose ring in 60° progressions in addition to one completed six-fold helix turn every 40.45 cm (14.7 Å). The angle of rotation of the C6 hydroxymethyl groups (χ_0) is set at 54° (54.1°). One ascending helix turn (yellow bonds,

Fig. 4) and one descending helix turn (white bonds) are immobilized on vertical 40.45 cm wooden dowels with a height difference of 6.6 cm (2.4 Å) and helix axis separation of 25.94 cm (9.71 Å). Bamboo skewers also form the hydrogen bonds (red), which, using the H-bond lengths of Table 10 of André, Mazeau et al. (1996), complete a bonding structure closely following that depicted in Fig. 11 of that paper.

2.4 In silico structural model

The model ('inulin molecule') corresponds to the inulin oligomer GF_8, incorporating the half unit cell plus terminal glucose and 2 spacer fructoses (Section 3.4). Geometry optimization and minimization use AMBER force field parameter version ff12SB (Case et al, 2012) and an initial steep descent down to 0.02 Å per step, followed by gradient minimization at that rate for 100 steps. This model is not subsequently relaxed After this, a glucose molecule is modelled to the C2 of the first fructose unit. In Fig. 5C, D, E, glucose is only modelled on chains Nos.1, 2, 3 and 4.

3. Results

3.1 Inulin crystal early development

Transmission electron micrographs (TEM) of MPI from stirred cool solutions show cleanly defined electron-translucent ovoids but resolve little structural detail. By contrast, freeze-fracture scanning electron microscopy (SEM) clearly shows laminar structures (Cooper & Petrovsky, 2011) and indeed inulin particles have other properties of classical thermoplastic polymers (Strobl & Schneider, 1980; Silvestre, Cimmino & Di Pace, 2002) including indications of spherulite growth patterns (polarized light microscopy: Hébette, Delcour, Koch, Booten & Reynaers, 2011). However, little can be deduced of surface structure. We accordingly followed early development of inulin crystals by AFM, in which a probe scans a surface to record fine detail (Section 2.2). We either sampled the course of crystallization for up to 5 days in repeated agitated runs at 5 °C (Fig. 1A, B, C) over a typical time course (Cooper et al. 2013), crystallized aliquots of such solutions on flat silicon wafers at RT (Fig. 1D), or examined washed, final preparations of delta inulin (Advax™, Fig. 1E, F). In suspension, rounded bodies occur at 24–48 h, somewhat indistinct as surface detail is obscured by glassy inulin after drying. Various fibrous forms are here abundant as bundles of finer flexible filaments, incomplete discs soon becoming more numerous. Any edges will be abraded by agitation effects, leaving rounded shapes. The discs later (> 48 h) assume dimpled appearances. Crystallization on surfaces (Fig. 1D) can produce flat spherulite-like forms with striated appearances suggestive of radial development as fibres. When finished as delta inulin (DI) the unobscured discoid surface resembles multi-layered, overlapping spherulites grown outwards in three dimensions from small central nuclei. Notably, among many different samples examined by us and others only one X-ray diffraction pattern is seen (Cooper et al., 2014b), and so there is no suggestion that these superficially different morphologies (fibre, discoid, spherulite) represent distinct phases but rather variations of the basic spherulite disc pattern. The fibres may be disc precursors or disturbed early forms of spherulites.

3.2 Rapid onset of inulin crystallization

Crystallization from inulin solutions can begin unexpectedly rapidly. Aggregation begins at a low 0.081 mg mL^{-1} (Dan, Ghosh & Moulik, 2009), while clear inulin solutions dissolved at 85 °C (DPn ~30, 100 mg mL^{-1}) stirred at 5 °C or 49 °C visibly nucleate (OD_{700} ~0.002) in 60–120 min (unpublished data). Frozen inulin solutions (50 – 100 mg mL^{-1}) very rapidly precipitate isoform types determined by the thaw temperature (Cooper et al., 2013). This also occurs in very dilute solutions (Fig. 2A). Thawing frozen clear solutions of dilute omega inulin (OI, DPn ~60, 0.5 mg mL^{-1}; Cooper et al., 2014b)) immediately precipitates inulin which then stabilizes within 15 min at 20 °C, or 3 min at 37 °C or 45 °C, to specific structures (Fig. 2B) with thermal properties of alpha-2 inulin, gamma inulin and DI, respectively. Here there appears a race between complete solution of a poorly crystallized/amorphous form and crystallization of a more temperature-stable form. Initiation of freeze-thaw precipitation is slowed by low levels of sucrose present during the thaw at hexose-to-hexose similar ratios (Fig. 2C), implying the key involvement of H-bond formation during initiation; glucose, fructose, xylose and glycerol were similarly inhibitory (data not shown) and so the effect is not specific to sucrose.

Unfrozen replicates at 0.5 mg mL^{-1} remain clear after 3 months at 5 – 37 °C, implying crystallization may depend on sub-microscopic crystal nuclei formed in transient saturated solutions as the thawing mass passes through its eutectic point. However, this can be very fast (time to complete thaw from −70 °C to ~5 °C < 60 s). The first melt (< 20 s) is very cloudy even while most remains frozen. The question is how very low levels (0.5 mg mL^{-1}) of two independent inulin chains of DPn ~60 can randomly fall into specifically ordered, complex structures in so short a time. Some form of rapid, specific initiation seems implicated as explored in the following sections.

3.3 Has glucose a role in inulin crystal structure?

Might inulin chains self-assemble rapidly because they have a specifically ‘sticky end’? In plant biosynthesis, fructose molecules are sequentially added to the fructose of a sucrose molecule (Franck & De Leenheer, 2002) and with few exceptions (De Leenheer & Hoebregs, 1994) the sucrose is retained intact. A heterologous terminal hexose (glucose) brings a novel aspect as André, Mazeau et al. (1996) expressly consider only poly [2 →1]-β-D-fructofuranan. ‘Sticky ends’ should include some extra affinity of glycosidic (terminal) glucose for fructose because in antiparallel duplexed chains glucose can only bond with fructose. Such bonding is found in sucrose crystals, where adjacent molecules are connected by four intermolecular H-bonds (O2g - O6f, O3g - O3f, O6g - O3g, O3f - O4f: Perez 1994). The two glucose-fructose links create a sucrose dimer by a close chelate-like dual H-bond that should be strong (Fig. 3) and that joins a chain of such dimers in the crystal. The two fructoses are in opposing orientation: they are in *obligate antiparallel alignment*.

We consider in what follows the proposition that inulin crystal initiation occurs by such fructose-glucose cross-linking. Such bonding would provide a nucleus to accelerate formation of the antiparallel helices proposed for inulin crystals, as amplified in Section 4. The presence of lesser polyhydric alcohols (sucrose, glucose, fructose, xylose, glycerol;

Section 3.2) would provide an obstacle to such interaction but their inhibition of crystallization does not indicate any specific location for the initial bonding.

3.4 Effect of proposed glucose cross-linkage on inulin structure – the physical model

A feasibility study using a ball-and-stick (non-space-filling; Section 2.3) physical scale model of the inulin monohydrate unit cell (replicating Fig. 11 of André, Mazeau et al., 1996) explores both its internal structural strengths and the steric acceptability of sucrose-like cross-linking. The model involves only one molecule of water of crystallization and hydrogen atoms are omitted for clarity. A further 11 molecules of water of crystallization are also omitted. In the inulin crystal, more support is provided by space-filling effects, adjacent unit cells and these extra water molecules, while in the model the correct dimensions are maintained by struts (Section 2.3). By 'best-fit' it is sterically feasible to insert a glucopyranose bridging via O6g-O2f, O3g-O3f provided the two fructose residues linked are those immediately below or above a unit cell in both chains. These two act as 'spacer' molecules.

The structure found is $(GF_8)_2$. The model's rear elevation shows the cross-link more clearly (Fig. 4A) but in this perspective view only some angles are accurately reproduced. In a front elevation of one workable arrangement of the isolated bridging structure (Fig. 4B) the glucose is covalently attached to one fructose as a normal, sucrose-like terminal glycoside, the other fructose receiving the H-bonding. The link is equivalent to the addition of one sucrose-fructose H-bonded dimer to either end of a unit cell. Only one basic architecture is feasible for the cross-link whether above or below the unit cell, although the tolerances in bond rotational angles and H-bond lengths allow some variation. Cross-H-bonding lengths of 2.5–3.5 Å between glucose and fructose are sterically acceptable, while the length shown is 2.5 Å. This compares with H-bond lengths in the rest of the unit cell of 2.5–3.4 Å (André, Mazeau et al., 1996) and with 2.8–2.9 Å in the sucrose crystal (Brown & Levy, 1973; Mathlouthi & Genotelle, 1998). The main rotational angles found are (at the glucose-fructose glycosidic link) gC2-gC1-gO1-fO2 = 10°, gC1-gO1-fO2-fC3 = 100°, and the H-bonded fructose C6 angle χ_0, fO5-fC5-fC6-fO6 = −160°, all with feasible tolerances of about ± 30°. Other glucose/fructose H-bonding patterns are not considered. The antiparallel nature of the two inulin chains is mandatory given the antiparallel orientation of the link.

The model of Fig. 4A is for illustration only, showing feasible linkage above or below a unit cell, as the second glucose unit is unlikely to link to the same chain in a polydisperse, long-chain sample (Section 4). Also the opposite-sense presentation of termini of geometry-minimized inulin chains (Section 3.5) would not normally favour this but there seems sufficient flexibility to allow the possibility.

3.5 In silico structural model

A single inulin chain with 8 fructose units (GF_8) is modelled *in silico* (Section 2.4) using known distances and angles of inulin monohydrate crystals to take account of intramolecular H-bonds (André, Mazeau et al., 1996) and the monoformat DPn data (Cooper et al., 2014b). This chain (degree of polymerization, DP, 9, 'inulin molecule') serves as an example for much longer isoform chains (DP >60) during feasible assembly into lamellar structures.

Stick and space-filled virtual diagrams (Fig. 5A, B) show the helical form of André, Mazeau et al., (1996) and the opposite-sense presentation of the glucose and fructose termini after minimization to optimize atom spacing.

Also following these authors, seven parallel inulin molecules in a hexagonal packing sheet simulate an inulin lamella, with alternate molecules 3, 4 and 5 aligned antiparallel. Fig. 5C looks along the helix axes of a stick diagram. While the AMBER force field is not suitable for modelling intermolecular H-bonding, the steric proximity of terminal glucoses and fructoses of antiparallel chains is demonstrated for upper and lower lamellar surfaces (Fig. 5D, E), and a feasible form of the actual bonding between chains of DP >20 is suggested in the physical model of Fig. 4. Such presentation and bonding can be repeated indefinitely (Fig. 5F) and the additional strength from the proposed glucose-fructose cross-links would favour extension length-wise to create fibres that could then bond laterally into lamellar spherulites (Section 3.1). This model treats chains of identical lengths but equally applies to non-identical chains (Section 4).

3.6 The crystal unit cell as the energetic unit

Fig. 6 interprets the unit cell (X to Y both ways) in rear elevation as in Fig. 4A, with the cross-links outside X and Y. In the unit cell itself, the two, opposite-sense glycosidic (helix) backbones with the hydrogen-bonding between them create three, interlocking ring-like structures (domains B, C, D) providing a sturdy, internal and self-sufficient lattice maintaining the unit cell's centre. However, the full strength of the unit cell requires building upon a preceding cell and beginning the succeeding one, thus adding a fourth and fifth ring domain E and A. Thus it is the *completion* of each unit cell both top and bottom that confers the full internal energetic quota of each unit. In a long, cross-linked pair of helical chains, domains A and E would merge and repeat many times but the glucose link only occurs at or near the terminus, where it can complete domains A or E.

Glucose cross-linking with a fructose of an adjacent chain is thereby proposed to start crystallization, increasing overall stability and in effect dictating the first ring domain. This process could in principle begin at either end but a top start would soon complete ring domain A (Fig. 6), rapidly followed by domain B and so need fewer residues to establish stability than a bottom start at domain E. Thus a top start should stabilise faster and so be favoured, when the last domain completed is E or E1 merged with A2, involving the most residues and largest energetic input.

4. Synthesis and Discussion

The crystalline portions of inulin isoforms differ by regular increments of one unit cell, comprising one complete turn of 6 fructose residues per chain in each of two antiparallel helical chains (Cooper et al., 2014b). Completion of each new structural unit 'locks in' the observed quantal increase in aggregate strength of H-bonding (Cooper et al., 2013). When considering the rapidity of specific inulin crystal initiation, in this study we asked whether the inulin terminal glucose could initiate crystallization by a glucose-fructose cross-H-bonding such as found in sucrose crystals. This would provide strong linking of two initially dissolved chains that would compel their antiparallel alignment. We find that such glucose-

fructose cross-linking is sterically feasible but would require two spacer fructose residues for the first such link, extra to the unit cell. Finishing a set of 5 internal H-bonding ring-domains would lock in energetic properties on *completion* of each unit cell, top and bottom.

Supporting this, inulin oligomers also evidence H-bond cross-linking. Uniquely confirming a stability point after completion of one unit cell, the steady drop in molecular optical rotation with increasing fructose content of all inulin oligomers from GF (sucrose) to GF_9 revealed a drastic difference in rate of change of rotation at GF_8 with changes in 3-H chemical shifts of all internal fructose, interpreted as abrupt changes to more rigid conformations (Oka et al., 1992). This is improbable in the absence of cross-linking. Single cross-links could produce stable, almost complete unit cells and two dimer structures identical to Fig. 4A, other types of cross-linked multimer being feasible. A minor optical rotation discontinuity at GF_4 coincided with stronger interaction of Ba^{2+} ions with inulin oligomers $GF_{3–5}$ than at other hexose ratios (^{1}H NMR spectroscopy: Timmermans et al., 1997), suggesting a cyclic structure analogous to cycloinulo-hexaose forming only at this level. These monodisperse samples have chains of very similar lengths where exact chain matching is frequent. Steric proximity in GF_8 preparations will encourage cross-linking of both termini that, once formed, would be more stable and eventually dominant.

Glucose initiation satisfactorily explains rapid, precise inulin crystallization. A glucose terminal group can feasibly seize a random fructose residue in another chain to form a strong cross-link. The antiparallel orientation of this glucose cross-link ensures that the seized chain must also be antiparallel, either before or as a result of the seizure. Just as a zip fastener requires exact initiation, so glucose initiation provides an exact start to the sequential formation of precisely located ring bonding-domains between two antiparallel inulin chains. These allow orderly formation of a series of exact bonding-domains more rapidly than random cross-linking and also ensure the fidelity between chains needed for long cross-linked stretches that explain the isoforms' thermal properties and the long rod-like helices required to form lamellae. We have noted (Cooper et al., 2014a) that single-hit gamma ray damage to MPI structures can be approximately halved by re-annealing surviving chains into the original type of structure, implying a pair-wise 'special relation' between chains. The bonding follows the chains, zipper-like, until meeting an anomaly. The looser structure near the Tc allows 'browsing' where even such complex bonding could travel along both chains until reaching stability, possibly by shortening un-duplexed regions.

How likely is the unoccupied terminal glucose on the initially seized chain to seize in turn a distal fructose of the first chain? We find this unlikely for polydisperse chains of 20-plus hexoses because of opposite-sense presentation, low steric proximity and many choices among competing chains. A looped, self-linking hairpin shape is similarly unlikely. Thus the seized chain is far more likely to extend to a third chain, eventually forming a monofilament associating laterally into a fibre then a lamella.

MPI's lamellar make-up is shown by SEM (Cooper & Petrovsky, 2011) and small-angle X-ray scattering (Hébette et al., 2011), further supported by crystal shape (André, Putaux et al., 1996) and spherulite format (Section 3.1). Dispersion of inulin in DMSO at 30 °C produces rod-shaped bundles (viscosity and TEM characteristics: Dan et al., 2009), and rope-like

structures are seen in freeze-thaw SEM (unpublished data). The most fitting picture of MPI seems a regular assembly of parallel, long rod-shaped helical polymers stacked with alternate antiparallel chains and axes perpendicular to the axes of long monofilaments each bonded laterally into fibres aligned radially in a lamellar plane and all assembled into multilayered spherulites. Such a model suggests equating lamellar thickness directly to isoform chain length but because hydration/volumes of aqueous MPI can vary 2.5-fold while retaining thermal properties of specific isoforms (Cooper & Petrovsky, 2011), this relation is obscured by unknown water dispositions.

As mentioned, any lateral bonding of the helices will preferably extend via an unrelated third chain, and the models in Figs. 4 and 5 will compel antiparallel alignment in entire alternate rows of new chains. While the first seizure to that second chain would require 2 spacer fructose units before unit cell assembly can begin, no such constraint applies to a second cross-link to a third chain because that link is not integral to unit cell development. A newly seized third chain (Fig. 5F) is free to begin its own unit cell duplex from its distal glucose and may well already have done so. Accordingly, the two spacer fructoses are only required for *alternate* glucose units. Unexpectedly confirming this, each isoform consistently involved only one ‘extra’ fructose per chain (Cooper et al., 2014b).

H-bonded water molecules also provide lateral bonding between adjacent helical duplexes (André, Mazeau et al., 1996). The two linked chains may be unequal lengths, and Hébette et al. (2011) have suggested an amorphous layer between lamellae following classical thermoplastic polymer theory (Strobl, 2007) that could comprise un-bonded ‘loose ends’ of inulin chains. Bond browsing should continue slowly until the duplex matures into the longest (most stable) cross-linked structure for the DP and temperature. Such slow, small transfer into higher isoforms is usual in long-term storage of inulin samples (unpublished data) and annealing is essential for stable monoformat preparation (Cooper et al., 2014b).

Other known properties of inulin isoforms follow readily from these concepts. Heat-conversion and spontaneous crystallization (Cooper et al., 2013), in both cases into specific isoforms at particular temperatures, are seen as re-arrangements of ring-bonding domains into new, longer structures more stable at the new, more disruptive environments (higher temperatures). Shorter chains not reaching this stability requirement are released into solution. The strictly polymorphic forms, where longer chains are assembled into lower phenotypes at lower energy environments, can be visualized to have shorter ring-bonded stretches which are then enabled by greater energy input (temperature) to browse into longer and more stable ring-bonded stretches. The aggregate number of these stretches determines the phenotype (Tc or MP).

5. Conclusions

We accordingly propose the structural concepts of glucose cross-link initiation, H-bonding ring-domain closure and progressive unit cell completion to account in molecular terms for all the known properties of the inulin isoforms, with additional glucose cross-linking at the distal termini accounting in part for lateral lamellar assembly.

Acknowledgments

We thank Dr Doug Taupin for invaluable support throughout the course of these studies. P.C. is an Emeritus Visiting Fellow of the Australian National University Medical School and of the John Curtin School of Medical Research, ANU, Canberra, Australia.

Funding

This project has been funded in whole or in part with Federal funds from the National Institute of Allergy and Infectious Diseases of the National Institutes of Health, under Contract No. HHSN272200800039C and Collaborative Research Contract No. U01AI061142. The content is solely the responsibility of the authors and does not necessarily represent the official views of the National Institute of Allergy and Infectious Diseases or the National Institutes of Health. This work was also supported by The Australian Research Council through a Linkage Grant (LP0882596) and by the South Australian Government through a Catalyst Research Grant.

Abbreviations

AFM	atomic force microscopy
DI	delta inulin
DP	degree of polymerization
DPn	number average degree of polymerization
MP	melting point
MPI	microparticulate inulin
OI	omega inulin
RT	room temperature (~20 °C)
SEM	scanning electron microscopy
TEM	transmission electron microscopy
Tc	critical temperature

References

André I, Mazeau K, Tvaroska I, Putaux JL, Winter WT, Taravel FR, Chanzy H. Molecular and crystal structures of inulin from electron diffraction data. Macromolecules. 1996; 29:4626–4635.

André I, Putaux JL, Chanzy H, Taravel FR, Timmermans JW, de Wit D. Single crystals of inulin. International Journal of Biological Macromolecules. 1996; 18:195–204. [PubMed: 8729031]

Barclay T, Ginic-Markovic M, Cooper P, Petrovsky N. Inulin – a versatile polysaccharide with multiple pharmaceutical and food chemical uses. Journal of Excipients and Food Chemistry. 2010; 1:1–24.

Brown GM, Levy HA. Further refinement of the structure of sucrose based on neutron diffraction data. Acta Crystallographica Section B. 1973; 29:790–797.

Case, DA.; Darden, TA.; Cheatham, TE., III; Simmerling, CL.; Wang, J.; Duke, RE.; Luo, R.; Walker, RC.; Zhang, W.; Merz, KM.; Roberts, B.; Hayik, S.; Roitberg, A.; Seabra, G.; Swails, J.; Goetz, AW.; Kolossváry, I.; Wong, KF.; Paesani, F.; Vanicek, J.; Wolf, RMJ.; Liu, X.; Wu, SR.; Brozell, RM.; Steinbrecher, T.; Gohlke, H.; Cai, Q.; Ye, X.; Wang, J.; Hsieh, M-J.; Cui, G.; Roe, DR.; Mathews, DH.; Seetin, MG.; Salomon-Ferrer, R.; Sagui, C.; Babin, V.; Luchko, T.; Gusarov, S.; Kovalenko, A.; Kollman, PA. AMBER 12. University of California; San Francisco: 2012.

Cooper PD, Barclay TG, Ginic-Markovic M, Petrovsky N. The polysaccharide inulin is characterized by an extensive series of periodic isoforms with varying biological actions. Glycobiology. 2013; 23:1164–1174. [PubMed: 23853206]

Cooper PD, Barclay TG, Ginic-Markovic M, Petrovsky N. Gamma ray sterilization of delta inulin adjuvant particles (AdvaxTM) makes minor, partly reversible structural changes without affecting adjuvant activity. Vaccine. 2014a; 32:552–557. [PubMed: 24342245]

Cooper PD, Barclay TG, Ginic-Markovic M, Gerson AR, Petrovsky N. Inulin isoforms differ by repeated addition of one crystal unit cell. Carbohydrate Polymers. 2014b; 103:392–397. [PubMed: 24528745]

Cooper PD, Petrovsky N. Delta inulin: a novel, immunologically-active, stable packing structure comprising β-D-[2→1] poly(fructo-furanosyl) α-D-glucose polymers. Glycobiology. 2011; 21:595–606. [PubMed: 21147758]

Dan A, Ghosh S, Moulik SP. Physicochemical studies on the biopolymer inulin: a critical evaluation of its self-aggregation, aggregate-morphology, interaction with water, and thermal stability. Biopolymers. 2009; 91:687–699. [PubMed: 19353642]

De Leenheer L, Hoebregs H. Progress in the elucidation of the composition of chicory inulin. Starch. 1994; 46:193–196.

Franck, A.; De Leenheer, L. Inulin. In: Vandamme, EJ.; De Baets, S.; Steinb chel, A., editors. Biopolymers. Vol. 6, Polysaccharides II: Polysaccharides from eukaryotes, Chapter 14. Berlin: Wiley-VCH Verlag GmbH; 2002. p. 439-479.

Gordon DL, Sajkov D, Woodman RJ, Honda-Okubo Y, Cox MM, Heinzel S, Petrovsky N. Randomized clinical trial of immunogenicity and safety of a H1N1/2009 pandemic influenza vaccine containing Advax polysaccharide adjuvant. Vaccine. 2012; 30:5407–5416. [PubMed: 22717330]

Hébette CL, Delcour JA, Koch MHJ, Booten K, Reynaers HL. Crystallization and melting of inulin crystals. A small angle X-ray scattering approach (SAXS). Polimery. 2011; 56:645–651.

Honda-Okubo Y, Saade F, Petrovsky N. Advax™, a polysaccharide adjuvant derived from delta inulin, provides improved influenza vaccine protection through broad-based enhancement of adaptive immune responses. Vaccine. 2012; 30:5373–5381. [PubMed: 22728225]

Larena M, Prow NA, Hall RA, Petrovsky N, Lobigs M. JE-ADVAX vaccine protection against Japanese encephalitis mediated by memory B cells in the absence of CD8+ T cells and pre-exposure neutralizing antibody. Journal of Virology. 2013; 87:4395–4402. [PubMed: 23388724]

Mathlouthi M, Genotelle J. Role of water in sucrose crystallization. Carbohydrate Polymers. 1998; 37:335–342.

Oka M, Ota N, Mino Y, Iwashita T, Komura H. Studies on the conformational aspects of inulin oligomers. Chemical and Pharmaceutical Bulletin. 1992; 40:1203–1207. [PubMed: 1394635]

Perez, S. The structure of sucrose in the crystal and in solution. In: Mathlouthi, M.; Reiser, P., editors. Sucrose, properties and applications. Berlin: Springer; 1994. p. 11-32.

Petrovsky N, Larena M, Siddharthan V, Prow NA, Hall RA, Lobigs M, Morrey J. An inactivated cell-culture Japanese encephalitis vaccine (JE-ADVAX) formulated with delta inulin adjuvant provides robust heterologous protection against West Nile encephalitis via cross-protective memory B cells and neutralizing antibody. Journal of Virology. 2013; 87:10324–10333. [PubMed: 23864620]

Saade F, Honda-Okubo Y, Trec S, Petrovsky N. A novel hepatitis B vaccine containing Advax, a polysaccharide adjuvant derived from delta inulin, induces robus humoral and cellular immunity with minimal reactogenicity in preclinical testing. Vaccine. 2013; 31:1999–2007. [PubMed: 23306367]

Silvestre, C.; Cimmino, S.; Di Pace, E. Morphology of polyolefins. In: Vasile, C., editor. Handbook of polyolefins, Chap. 7. CRC Press Technology of Engineering, Marcel Dekker; New York: 2002. p. 175-205.

Strobl GR, Schneider M. Direct evaluation of the electron density correlation function of partially crystalline polymers. Journal of Polymer Science: Polymer Physics Edition. 1980; 18:1343–1359.

Strobl, GR. The physics of polymers: concepts for understanding their structures and behaviour. Berlin: Springer; 2007.

Timmermans JW, Bitter MGJW, de Wit D, Vliegenthart JFG. The interaction of inulin oligosaccharides with Ba^{2+} studied by ^{1}H NMR spectroscopy. Journal of Carbohydrate Chemistry. 1997; 16:213–230.

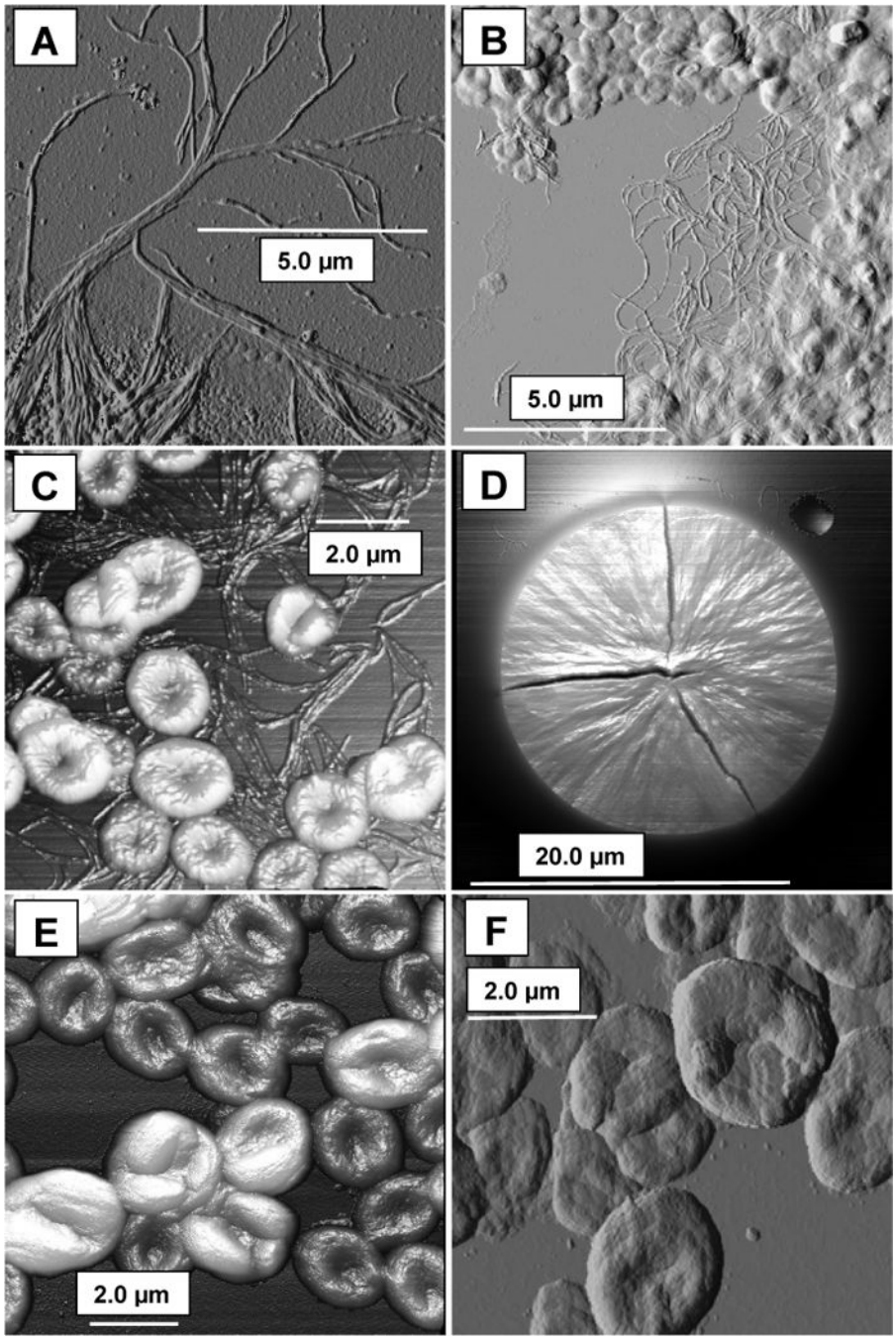

Fig. 1. Particulate forms detected by atomic force microscopy during crystallization of inulin solutions

A, B, C: fibrous forms and rounded bodies at 24 – 48 h; **D:** spherulite grown on a flat surface, the cracks being drying artefacts; **E, F:** final forms of delta inulin at ~8 days. **C, D, E** used the 3-D facility of the AFM software, where more elevated features appear brighter. The bars show scale.

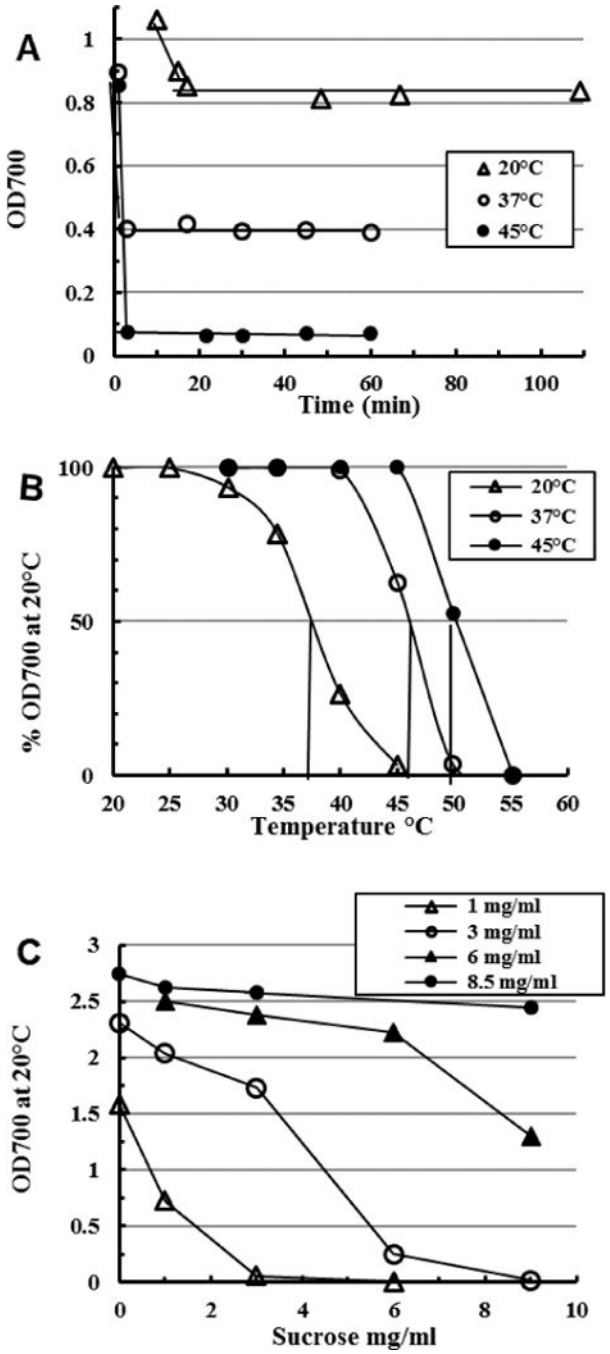

Fig. 2. Rapid assembly of specific structures on freeze-thaw crystallization of very dilute inulin solutions

Omega inulin (DPn ~60) at 0.5 mg mL^{-1} was dissolved at 85 °C and 5 mL aliquots frozen in thin-walled glass tubes to −70 °C. At zero time aliquots were agitated in well-circulated baths at 20 °C, 37 °C and 45 °C and (**A**) the OD_{700} read as soon as ice disappeared and at later intervals; (**B**) when stable (5–20 min), the OD_{700} of another aliquot from each bath was read at increasing temperatures in the standard OD_{700} thermal transition assay (Cooper et al., 2013). (**C**) similar test in which dilutions of dissolved OI (legend) frozen to −70 °C in

presence of the indicated concentrations of sucrose were thawed (10 min, 20 °C) and the OD_{700} read at once. Readings were stable for 1 h but increased 10–50% over 6 days with negligible relative change.

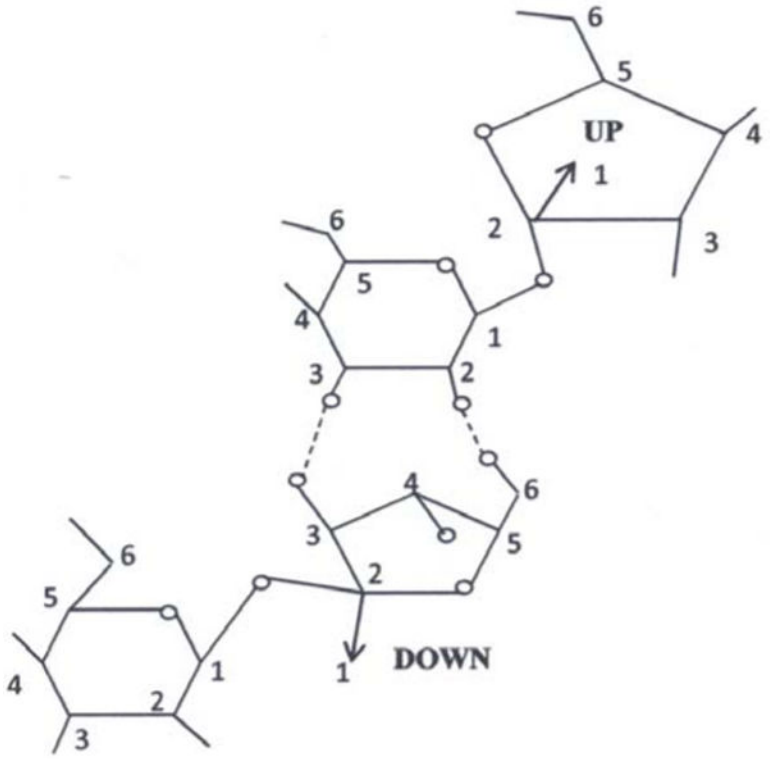

Fig. 3.
Fructose-glucose hydrogen bonding between sucrose crystal molecules. (Perez, 1994).

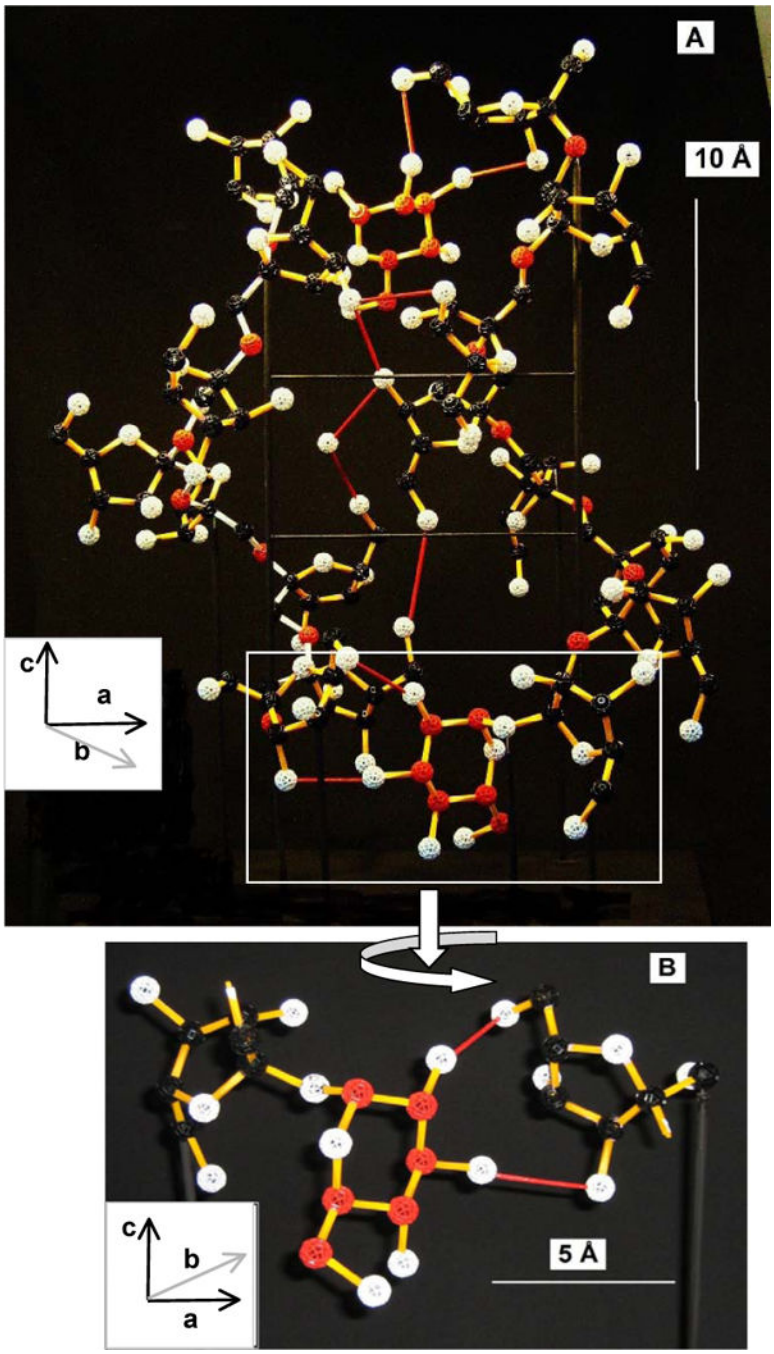

Fig. 4. The physical model of the inulin unit cell

The proposed glucose cross-link is included. Colour key: glucose C (red), other C (black), glycosidic O (red), other O (white), H omitted, ascending inulin helix bonds (yellow), descending helix (white), H-bonds (red), all other bonds (yellow). Insets show axis orientations using the convention of André, Mazeau et al. (1996). **A:** Rear elevation; **B:** Enlargement of the lower bridging structure from the boxed area in Fig. 4A (front elevation). The bars show scale.

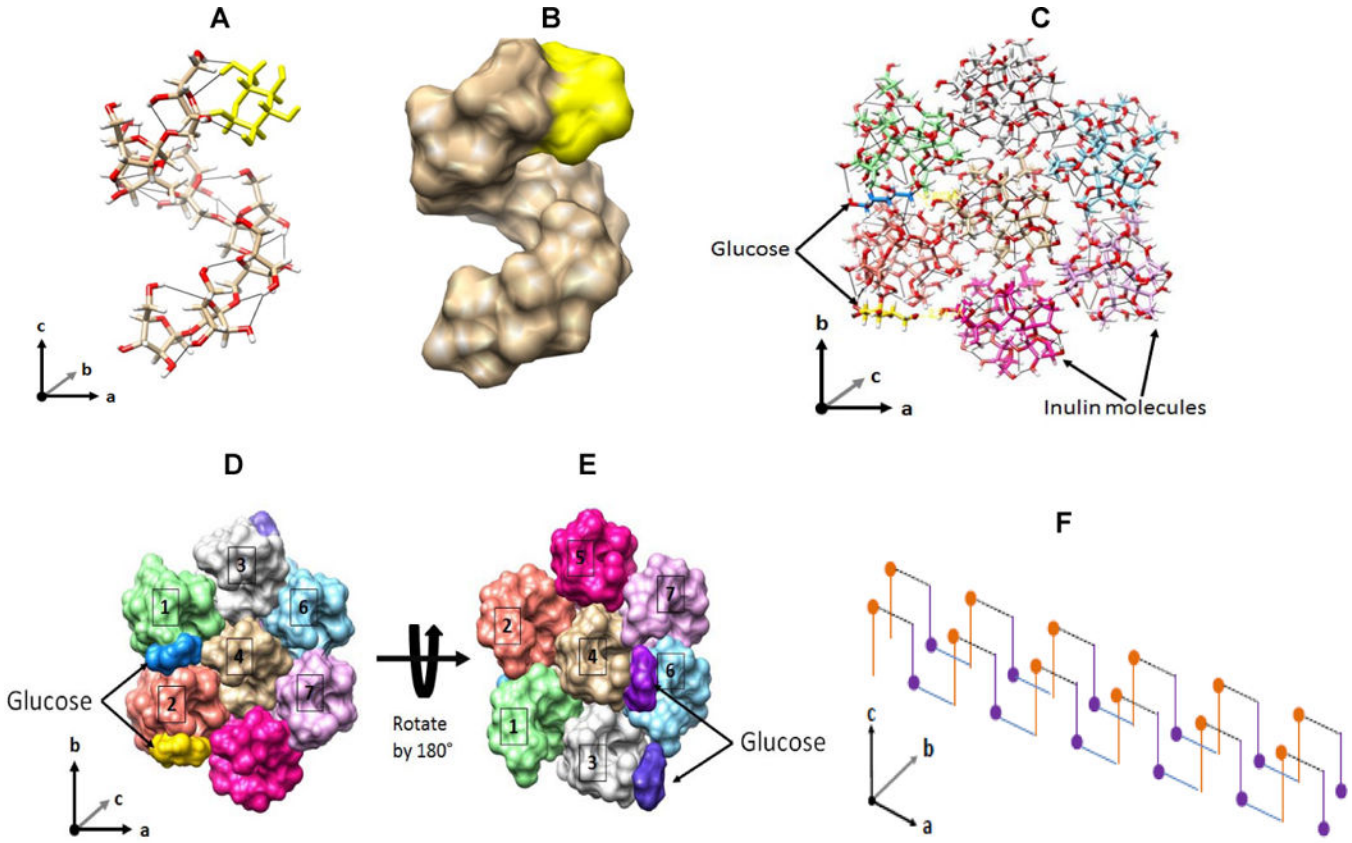

Fig. 5. ***In silico*** **relation of inulin molecules**

'Inulin molecule' (GF_8): **A,** stick diagram: O (red), C (grey), H (white), glucose (yellow), intramolecular H-bonds black lines; **B,** space-filled diagram: electron spaces of fructose (grey) and glucose (yellow). *Hexagonal packing of seven inulin molecules:* **C**, stick diagram (top); **D** space-filled diagrams, top, **E** ditto under, 180° rotation of D. Inulin molecules have different colours while glucose has blue and yellow (arrows). H-bonds are black lines. Molecules No.3, 4 and 5 are antiparallel. *Glucose cross-linking proposed:* **F**, Terminal glucoses (dots) H-bond with distal fructoses of antiparallel molecules (purple), and cross-linking repeated forming an unlimited rod or, with lateral H-bonding, a lamellar multimer.

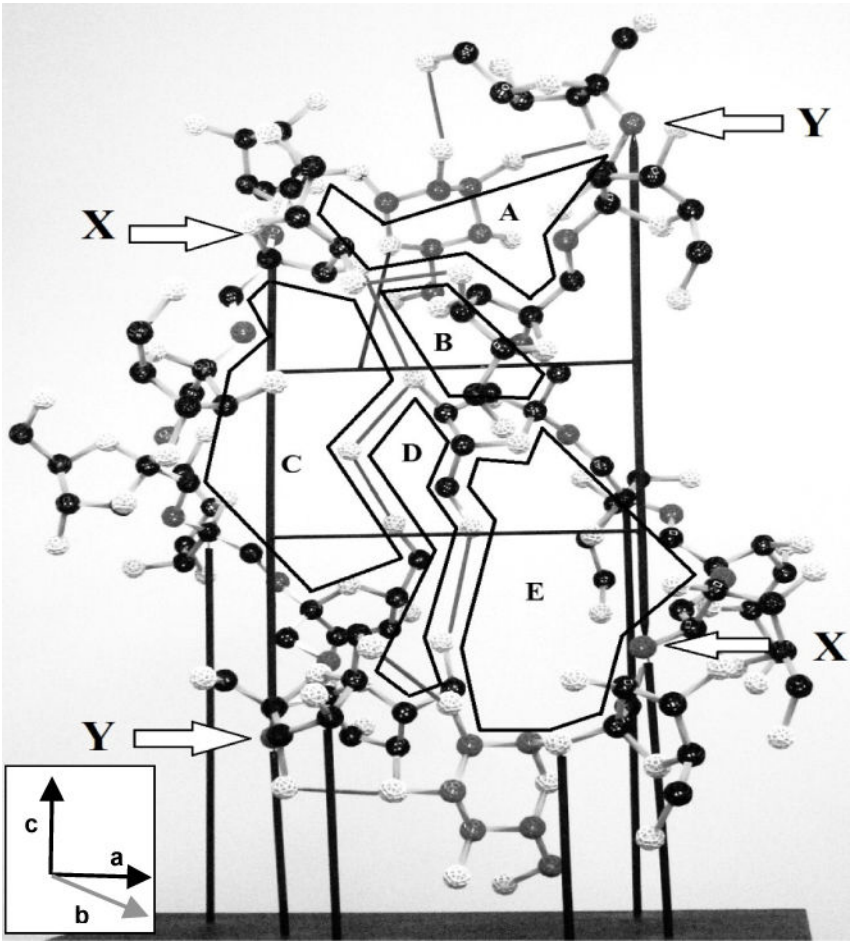

Fig. 6. Diagrammatic outline of the ring-bonding domains of the inulin unit cell (rear elevation, as in Fig. 4A)

Inset shows axis orientation using the convention of André, Mazeau et al. (1996). The diagram includes the proposed glucose bridging structures (Fig. 4B) to illustrate completion of domains A and E.